Catalysis Science & Technology

PAPER

View Article Online
View Journal | View Issue

Cite this: *Catal. Sci. Technol.*, 2016, **6**, 2742

Framework-substituted cerium MCM-22 zeolite and its interlayer expanded derivative MWW-IEZ†

Wieslaw J. Roth,[a] Barbara Gil,*[a] Wacław Makowski,[a] Andrzej Sławek,[a] Aleksandra Korzeniowska,[a] Justyna Grzybek,[a] Michał Siwek[a] and Piotr Michorczyk[b]

Received 30th November 2015,
Accepted 2nd March 2016

DOI: 10.1039/c5cy02074c

www.rsc.org/catalysis

Framework-substituted cerium MCM-22 zeolites were synthesized with both TEOS and solid silica sources. The Si/Al ratio in the gel was 15/1 with two different Si/Ce ratios equal to 100/1 and 30/1. The products showed high Brønsted acid site concentrations, above 700 μmol g^{-1}, that diminished slightly as the Ce content increased. The state of Ce was evaluated by IR and UV-vis spectroscopy. There was no indication of a separate Ce phase and extraframework atoms. Both oxidation states, 3+ and 4+, were present. In contrast to the interlayer expanded form MCM-22-IEZ with Ce exchanged into it, the present MCM-22 did not show oxidation of adsorbed CO. This indicates fundamental differences in the location of Ce, which is outside the framework in the exchanged form. The framework-substituted Ce-MCM-22 became active for CO oxidation after its conversion into the IEZ form and additional exchange of Ce. Textural properties were evaluated by nitrogen adsorption and quasi-equilibrated temperature-programmed desorption and adsorption (QE-TPDA) of hydrocarbons.

Introduction

Microporous materials, such as zeolites[1,2] and related structures,[3] can incorporate various metal atoms in their frameworks with creation of valuable centers for catalytic reactions.[3–5] The foremost example is aluminum, which produces strong acid sites in zeolites as it generates negative charges in the framework.[6] As strong solid acids, zeolites are particularly useful for selective hydrocarbon conversions[7,8] and are widely used as catalysts in the petroleum and chemical industries.[9,10] Transition metals can introduce other types or complementary functionalities in zeolites, especially for redox reactions.[11,12] This is exemplified by substitution of Ti into the MFI framework, which produced an extraordinary oxidation catalyst TS-1.[13,14] It resulted in broader interest in transition metal-functionalized zeolites and related materials.[15–17] Al is unique and different from the majority of other elements that can functionalize frameworks because it can be readily incorporated in large amounts, up to a Si : Al ratio of 1 : 1 depending on a particular structure.[18] Transition metal atoms are typically more difficult to insert into zeolite frameworks and usually in the amount of only up to a few percent content. They often form a separate phase when a higher amount is attempted. The reasons for this incompatibility are not well known but typically involve size, charge and unfavorable chemistry and solubility.[18]

Rare earth elements made a special contribution to zeolite catalysis as they enabled the first application in the 1960s. They were found to stabilize and activate zeolite Y upon exchange into the pores producing an extraordinary cracking catalyst,[19] thus demonstrating the potential of zeolites for catalytic conversion of hydrocarbons. This led to the first and the largest scale application of zeolites in industrial catalysis[20] stimulating subsequent great expansion and development that is still continuing today. It has been marked by many breakthroughs and valuable achievements with other zeolites also showing extraordinary performances.[21]

The exchange of rare earth ions having a 3+/4+ charge into zeolite Y has been possible because of its high Al content producing sufficient charge density combined with large pores (0.74 nm) in the framework. Other valuable zeolites usually contain much less Al and have smaller pores, which often thwarts significant exchange of these cations. Similarly, incorporation of lanthanide atoms (Ln) into zeolite frameworks has not been very effective either.[17,19] This may be changing now due to recent promising leads developed with zeolite MWW for both enhanced exchange[22] and framework substitution of Ln metals.[23] These findings are of considerable interest because MCM-22 is a unique[24] and valuable commercial catalyst.[25,26] It is also special as a prominent representative of 2-dimensional (2D) zeolites.[27] It readily produces

[a] *Faculty of Chemistry, Jagiellonian University in Kraków, Ingardena 3, 30-060 Kraków, Poland. E-mail: gil@chemia.uj.edu.pl; Fax: +48 12 634 0515; Tel: +48 12 663 2016*
[b] *Faculty of Chemical Engineering and Technology, Cracow University of Technology, Warszawska 24, 31-155 Kraków, Poland*

† Electronic supplementary information (ESI) available. See DOI: 10.1039/c5cy02074c

various layered forms, which are important on their own but can be also modified post-synthesis to obtain more open structures like pillared, delaminated and interlayer expanded (IEZ) species.[27] In fact, the enhanced Ce exchange into MCM-22 became possible upon its transformation into the expanded IEZ form with enlarged interlayer pores.[22] The increased Ce uptake resulted in activation for CO oxidation, which was negligible with the standard MWW zeolite containing less Ce.

The present study concerns the second case, *i.e.* framework-substituted lanthanide MCM-22, which has been reported recently[23] and can be considered as a significant innovation. The synthesis entailed a novel approach involving the use of a liquid silica source, *i.e.* tetraethyl orthosilicate (TEOS), which facilitated the formation of an intimate mixture with lanthanide ions by 'co-hydrolysis in an acid medium'. After addition of the remaining ingredients, the gel was crystallized by standard hydrothermal synthesis in a basic medium. The following evidence was provided to support the postulated incorporation of Ln ions in the framework: (i) apparent expansion of the unit cell by up to 1.5% in comparison to the Ln-free parent zeolite, (ii) increased content of the template (hexamethyleneimine, HMI) suggesting the neutralization of additional negative charges due to Ce/La in the 3+ state, (iii) 4–5 cm^{-1} downward shift of the Si–O–Si IR band apparently due to Ce/La incorporation; the shift was not observed when metals were impregnated/exchanged, (iv) UV-vis bands at about 300 nm and lower, assigned to tetrahedral lanthanide atoms, (v) upfield shift of ^{29}Si NMR peaks and 'apparent overlap of the bands in the Q^4 range for Ce-MCM-22 due to an (unspecified) paramagnetic effect', and (vi) catalysis – hydroisomerization of *n*-heptane showing an increase in conversion by up to two times in bimetallic Pt–lanthanide–MCM-22.

The reported synthesis of Ln-MCM-22 zeolites raises many interesting possibilities for study and further development. This work is focused on obtaining additional vital information related to catalysis, namely the nature and concentration of acid sites and CO oxidation. The former was not investigated in the first study. The latter has been demonstrated by MWW materials with Ce introduced by exchange and thus being in extraframework positions. These characterization studies are reported in the context of comparing the products obtained by using TEOS and solid silica. This is of interest for both fundamental and practical reasons. The use of TEOS in the original work was crucial for obtaining maximum dispersion of lanthanide ions in the silica matrix.[23] So the question is how the synthesis is affected by TEOS replacement with alternative reagents, like solid silica. This is hardly an exercise in screening various silicas because TEOS is uniquely disadvantaged among common silica sources for reasons of cost, special handling required to avoid hydrolysis, and health and safety issues. Even at a laboratory level, it is less convenient as it requires additional steps: ethanol evaporation and weight adjustment. We found that the properties of products obtained with fumed silica did not deviate too much, if at all, from those derived from TEOS. The practical benefits are further discussed in the Results and discussion section. We also studied the synthesis of IEZ derivatives[28] and their behavior towards CO oxidation.

Experimental

The starting MCM-22P materials were synthesized with TEOS and fumed silica from gels having molar ratios of Si/Al = 15 and Si/Ce = 100 and 30. The reagents for syntheses were obtained from Aldrich. The composition of sodium aluminate $NaAlO_2$ (Riedel-de Haen) was assumed to be 53% Al_2O_3 and 42.2% Na_2O. The amounts used to prepare the synthesis gels are listed in Table 1 and correspond to the following compositions: $x\mathrm{Ce}:\mathrm{SiO_2}:0.25\mathrm{NaOH}:0.033\mathrm{Al_2O_3}:0.6\mathrm{HMI}:20\mathrm{H_2O}$ (x = 0.01 and 0.033). The acid/anion contribution from Ce salts is small and is not included in the calculations.

Cerium nitrate was dissolved in 0.3 M HCl. After addition of the silica source, the mixture was heated at 90 °C for 2 h. Ethanol generated due to TEOS hydrolysis was distilled off. The slurry was weighed and the amount of water was adjusted as needed for the next steps. Subsequent additions included HMI, NaOH and sodium aluminate dissolved in water. The gel was mixed for 20 h and then heated in a Teflon-lined autoclave at 165 °C for 6 days without agitation (static). The products were recovered by standard methods and dried at room temperature overnight. The preparations with solid silica were carried out both with and without the use of acid solution at the beginning, *i.e.* cerium nitrate was dissolved in acid and water, respectively.

X-ray powder diffraction (XRD) measurements were carried out using a Philips X'Pert diffractometer APD with CuKα radiation (λ = 0.154 nm) in the 2θ range of 5–50° with steps of 0.02°.

The Ce, Al and Si content was measured for the calcined samples using a Thermo Scientific ARL Quant'x EDXRF analyzer.

Nitrogen adsorption isotherms were determined by the standard method at −196 °C (liquid nitrogen temperature) using an ASAP 2025 (Micromeritics) static volumetric apparatus. Before adsorption, the samples were outgassed at 350 °C using a turbomolecular pump to remove adsorbed water.

SEM images were obtained using a Tescan Vega3 LMU microscope with a LaB_6 emitter (voltage of 30 kV). Samples were coated with gold before imaging.

UV-Vis-DRS spectroscopy for the study of coordination, oxidation states and aggregation of cerium in the MWW zeolites was carried out using an Evolution 600 (Thermo) spectrophotometer. The measurements were performed at room temperature in the range 200–900 nm with a resolution of 2 nm.

IR spectra in the ATR mode were recorded on a Bruker Alpha spectrometer equipped with a single reflection diamond ATR module and a DTGS detector, working with a spectral resolution of 4 cm^{-1}. The ATR spectra were normalized to the

Table 1 The amounts of reagents (in grams) used to prepare the synthesis gels

Reagents	Ce-T-100	Ce -T-30	Ce-A-100	Ce-A-30	Ce-A-30-no acid	MCM-22-A
TEOS	22.62	18.86	—	—	—	—
Aerosil 200	—	—	6.04	6.06	6.02	6.00
0.3 M HCl	20.54	17.42	17.08	17.16	—	—
$Ce(NO_3)_3{\cdot}6H_2O$	0.46	1.30	0.38	1.30	1.30	—
HMI	6.46	5.50	5.48	5.48	5.47	5.50
$NaAlO_2$	0.68	0.58	0.56	0.58	0.58	0.58
50% NaOH	1.42	1.30	1.26	1.29	1.25	1.25
H_2O	22.08	25.64	25.62	25.65	35.74	42.70

intensity of the 800 cm^{-1} band, characteristic of T–O internal vibrations.

The acidity and degree of cerium oxidation were investigated by FTIR spectroscopy based on adsorption of pyridine and CO used as probe molecules. The accessibility of the acidic centers was measured using *tert*-butylnitrile (pivalonitrile, PN). The samples were activated in the form of self-supporting wafers for 1 hour at 470 °C prior to the adsorption of probe molecules at the following temperatures: 170 °C for pyridine (POCh Gliwice, analytical grade), room temperature for pivalonitrile (Sigma Aldrich, ppa) and −100 °C for CO (Linde Gas Polska, 99.95% used without further purification). The spectra were recorded with a Bruker Tensor 27 spectrometer equipped with an MCT detector and working with the spectral resolution of 2 cm^{-1}. All spectra presented in this work were normalized to the standard 10 mg pellet (density of 3.2 mg cm^{-2}) and the accuracy of normalization was verified by comparing the overtones for all samples. The concentrations of Lewis and Brønsted acid sites were calculated using previously reported absorption coefficients[29] ε(LAS) = 0.165 cm^2 μmol^{-1} and ε(BAS) = 0.044 cm^2 μmol^{-1} and the intensities of the corresponding pyridine maxima after pyridine was desorbed at 250 °C to ensure complete removal of weakly adsorbed species.

For detailed porosity analysis of the studied zeolites, quasi-equilibrated temperature-programmed desorption and adsorption (QE-TPDA) of hydrocarbons was employed.[30,31] QE-TPDA measures the amount of sorbate desorbed or adsorbed by a sample as a function of temperature which is changing cyclically. QE-TPDA measurements of hexane, cyclohexane and nonane were performed with the use of a thermodesorption apparatus equipped with a thermal conductivity detector (Micro Volume TCD, Valco). Prior to the QE-TPDA experiment, a sample (*ca.* 6–10 mg) was activated by heating in He flow (10 °C min^{-1} to 500 °C). The initial adsorption was carried out at room temperature by replacing pure helium used as the carrier gas with helium containing a small admixture of a hydrocarbon (*ca.* 0.4 vol%). After adsorption was completed, the QE-TPDA experiment was performed by cyclic heating and cooling of the sample (10 °C min^{-1} to 400 °C) in He/hydrocarbon flow (6.5 cm^3 min^{-1}). The desorption–adsorption cycles were separated by 1 h isothermal segments at room temperature. The micro- and mesopore volume calculations were carried out by integration of the experimental desorption maxima and adjustment based on the calibration data. The density of the adsorptives was assumed to be equal to that of the liquids (0.659 g cm^{-3} for hexane, 0.718 g cm^{-3} for nonane and 0.7781 g cm^{-3} for cyclohexane). High-purity hydrocarbons delivered by Sigma-Aldrich were used without additional purification.

Results and discussion

The MCM-22P preparation selected for this work had high Al content with Si : Al equal to 15/1 in the gel. It was chosen in order to maximize the acid site concentration and potential catalytic activity. Two nominal Ce contents were targeted: 100/1 and 30/1 Si/Ce molar ratios. The preparations were carried out with TEOS and fumed silica with addition of Ce nitrate in an acid medium. In addition, the preparation of the starting silica/cerium mixture was also carried out in water, designated as 'no acid' synthesis. The properties of the products are summarized in Table 2.

The substitution of TEOS with fumed silica produced MCM-22P with comparable X-ray diffraction and textural properties but with slightly lower Ce content. This difference may be within the accuracy of the measurements or be caused by some chemical factors during synthesis but they are unknown yet. If the observed lower Ce content in the Aerosil preparations is real, it can be increased by starting with a higher initial amount of the Ce salt. Based on this, we consider both these types of preparations to be equivalent.

Table 2 Basic properties of the studied MCM-22 zeolites in their calcined form; T and A are TEOS and Aerosil preparations; 'no acid' denotes syntheses without the use of acid medium for cerium nitrate dissolution, IEZ denotes Interlayer Expanded Zeolite and Ce at the end of the name denotes additional ion-exchange of cerium cations

Sample	Ce, wt%	Al_2O_3, wt%	Si/Al (XRF)	Si/Ce (XRF)	BAS, $\mu mol\ g^{-1}$	LAS, $\mu mol\ g^{-1}$
Ce-T-100	2.18	6.58	11	94	842	99
Ce-T-30	4.27	8.24	9	45	764	61
Ce-A-100	1.64	9.47	8	119	971	59
Ce-A-30	3.09	9.20	8	63	892	32
Ce-A-30-no acid	4.98	7.99	14	24	928	67
Ce-A-30-no acid-IEZ	0.83	4.10	19	257	492	129
Ce-A-30-no acid-IEZ-Ce	3.56	2.65	15	57	492	139
MCM-22-A	0	5.21	15	—	892	51
MCM-22-A-IEZ	0	4.91	16	—	514	145

The viability of TEOS replacement with solid silica in making Ln-MCM-22 zeolites has non-trivial practical benefits. It simplifies the synthesis by eliminating the ethanol evaporation step. TEOS is a very expensive and inconvenient silica source that has to be avoided if possible. It can be degraded by hydrolysis during storage and handling and represents a health hazard if inhaled. The handling and safety problems increase with the scale of preparations and for industrial application of the present materials the replacement of TEOS with different silica would be the primary objective.[10] The use of TEOS is possibly acceptable for the manufacture of the Ti-MFI, TS-1,[13] which is a high-value unique product manufactured on a relatively moderate scale. However, even in this case, the replacement with alternative inorganic silicas appears to be an ongoing effort.[16] The present result is also noteworthy because the use of TEOS to generate an intimate mixture with lanthanides was considered a key component of the synthesis strategy. It is possible that fumed silica can also produce similar homogeneous mixtures or, alternatively, the underlying mechanism is more complex than that initially envisioned. Additional syntheses were carried out without the initial digestion of silica and the Ce salt in an acid medium. The detailed overview and analysis of the results are discussed below.

The central issue of framework substitution of Ce is confirmed by the similarity of the synthesis and product properties to the original report by Wu *et al.*,[23] the absence of Ce compounds as a separate phase and the different behavior in comparison to Ce introduced by exchange (spectroscopic features, oxidation of CO). Additional evidence was obtained based on the experiments of pyridine adsorption, which are discussed in detail below.

1. X-ray diffraction and confirmation of the MCM-22P structure of the preparations

The XRD patterns shown in Fig. 1 confirm that the as-synthesized products are layered precursors MCM-22P with high crystallinity. This conclusion is based on the series of diagnostic reflections, recognized and reported previously, at the following positions (identified by (*hkl*) indices and 2Θ degrees (°) of Cu Kα radiation used throughout): (002), 6.5°; (100), 7.1°; (101), 8°; (102), 9.8°; (220), 25°; (310), 26°. The distinct doublet visible at 6.5–7.1° proves that the product is MCM-22P and not the 3D framework (MCM-49), which would show only a single peak at 7.1°. This is important for post-synthesis modification, which is not possible with the latter. We did not attempt to determine the unit cell constants and evaluate volume expansion, which the original study reported as one of the indications of Ce incorporation into the framework. The maximum expansion of the unit cell volume due to Ln insertion was said to be equal to 70 Å^3 corresponding to about 1.5% of the original volume (4630 Å^3) determined for MCM-22 without these metal atoms. This value may be within the accuracy of routine XRD determinations in both studies, the present and previous, especially when looking at the quality of the patterns, which are not in high resolution.

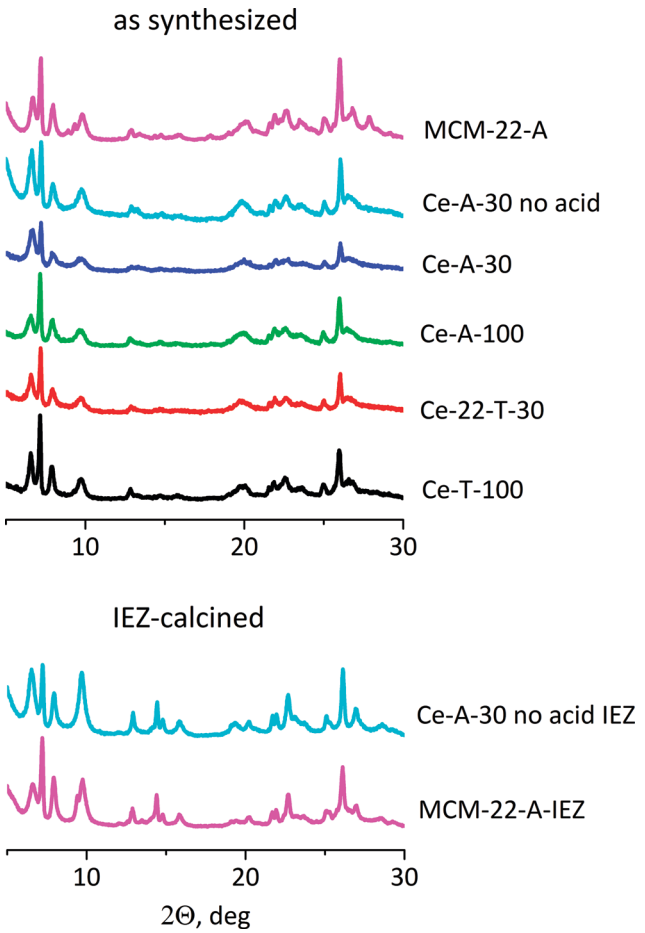

Fig. 1 XRD patterns of the Ce-MWW zeolites under study.

Better quality and accuracy is possible but it requires specialized equipment and methodologies. Furthermore, it has not been shown conclusively for zeolites in general that metal incorporation can be correlated with unit cell expansion, except for some really unique cases like Al content in zeolite faujasite. No other crystalline phases are evident except for additional small peaks in MCM-22-A at 8–9.6° and around 2Θ = 28°, and also below 9.6° for MCM-22-A-IEZ. They are probably due to a small amount of impurities. These samples are not of primary interest here as they were made only for comparison with the Ce preparations. The synthesis was simply based on not adding the Ce salt and may not reflect an optimal procedure. Overall, good veracity of the preparations can be claimed based on the results from powder crystallography.

The SEM images (Fig. 2) show the crystal morphology of Ce-MCM-22 zeolites obtained with TEOS and Aerosil as silica sources. The morphology is also the same for the preparation without the use of an acid for cerium nitrate dissolution and is retained after the silylation procedure.

2. IR and skeletal vibrations

The skeletal vibrations of all MCM-22 samples, both with and without Ce, look very similar and analogous to those of unmodified MCM-22, confirming the presence of the main

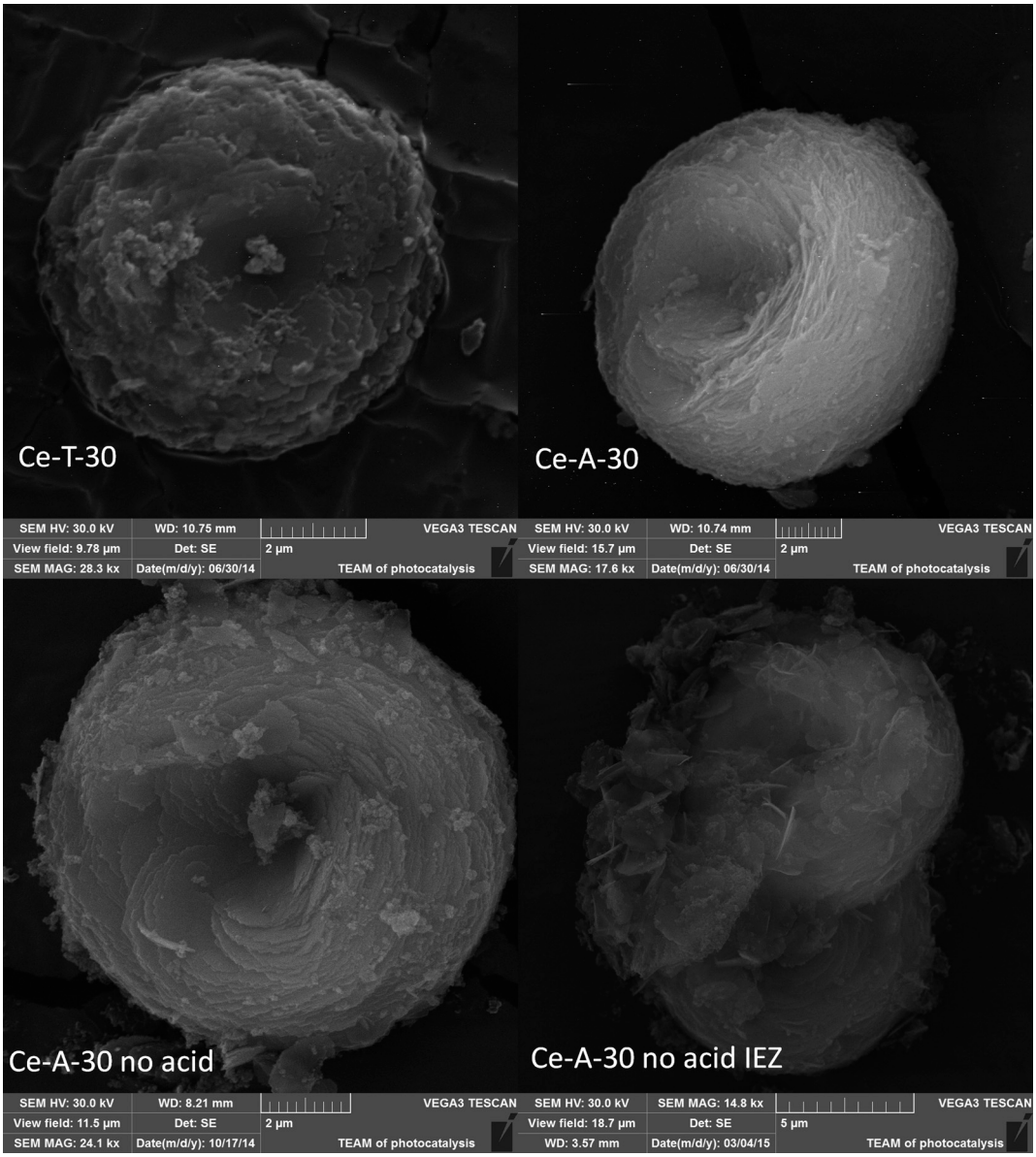

Fig. 2 SEM images of the Ce-MWW zeolites under study.

structural features of the MWW framework (Fig. 3). The positions and half-widths of the main IR maxima at *ca.* 1015 cm^{-1} (ν_{asym} T–O internal vibrations) and 1070 cm^{-1} (ν_{asym} T–O external vibrations) do not change significantly with the change of the silica source or cerium content. Variations in the frequency of the band of ν_{asym} T–O internal vibrations were claimed in the original work as evidence of cerium incorporation in the framework. However, the observed shifts are below 5 cm^{-1} and, considering their substantial half-widths (125 cm^{-1}), this evidence must be viewed as inconclusive. Additionally, Sousa-Aguiar *et al.* observed[32] that the frequency of the band attributed to the asymmetric stretching of the TO_4 tetrahedra continuously shifted to higher wavenumbers with the exchange of sodium for rare earth cations. The intensity of the double band at 595 and 545 cm^{-1}, which is characteristic of double-six-ring (D6R) vibrations, is also practically the same for all samples confirming good and comparable zeolite framework quality of all materials.

3. Metal incorporation

The basic composition information in terms of Si/Al and Si/Ce ratios was obtained with the calcined materials by XRF analysis and the values are listed in Table 1. The actual Si/Al values are believed to be somewhat higher than those measured by XRF based on experience during earlier studies. The Si/Ce ratios are close to the nominal values for the '100/1' preparations but significantly higher than those with the '30/1' ratios, suggesting incomplete Ce incorporation. In general, one expects that all Al and Ce present in a gel end up in the final solid product under high pH conditions. On the other hand, the determined acid site concentration also favours the indication of a lower degree of Ce incorporation in the solid silica

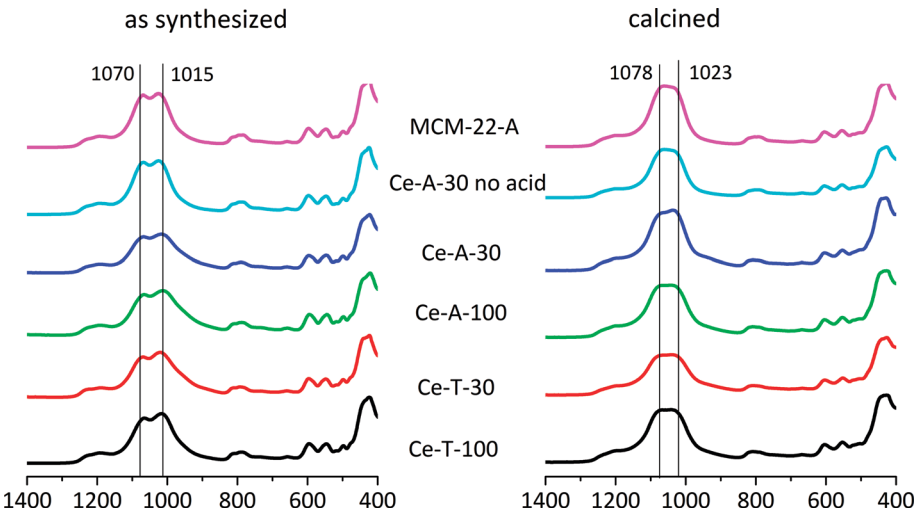

Fig. 3 IR spectra in the ATR mode of the MWW zeolites under study. Spectra normalized to the integrated intensity of the band at 800 cm^{-1}.

syntheses. As is mentioned, this may not present a practical problem since the lower Ce content/incorporation in the non-TEOS synthesis can be remedied by simply starting with a higher metal content in the gel.

The preparation without acid hydrolysis of silica and cerium gave a product with higher cerium content and Brønsted acidity. This indicates that digestion in an acid environment may not be necessary, but the BET surface area was lower in comparison to that of the preparation with acid hydrolysis. These trends suggest opposite effects on the quality of the product and the question of optimum synthesis remains open.

4. Acid site concentration

The obtained Ce-MCM-22 zeolites showed high values of Brønsted acid site concentration (BAS, approaching 1000 μmol g^{-1}, based on pyridine adsorption followed by FTIR). This is only slightly below the highest values reported for MWW materials equal to about 1200 μmol g^{-1}, which reflects the maximum Al content possible in the layer, *i.e. ca.* 5–6 per unit cell.[29] The concentration of BAS decreases as the amount of Ce increases, which in this case occurred in two ways: Si/Ce of the synthesis mixture was changed from 100/1 to 30/1 and for TEOS and fumed silica preparations with the same Si/Ce in the synthesis mixture the former ended up with higher Ce content in the product and showed lower BAS values. This trend cannot be explained as a simple neutralization process by Ce cations, because no Ce was detected in extraframework positions (*vide infra*). In general, there is the possibility for complex interactions and dependencies among various components: Al, Ce and the framework. The state and behaviour of Ce atoms are particularly difficult to elucidate, especially because they are found in both 3+ and 4+ states, as demonstrated later in the discussion. The latter does not contribute acidic OH groups in tetrahedral coordination. The amount of Lewis acidity (LAS), which can be a measure of defects and deviation from an ideal zeolite framework, is quite low and should be viewed as a positive sign. If cerium was present at the exchangeable/extraframework positions, it would be detected by pyridine, giving a specific maximum at 1442 cm^{-1} (ESI,† Fig. S1). The high values of Brønsted acid site concentration determined by pyridine adsorption are confirmed in the region of OH vibrations. The qualitative and quantitative features of the profiles are characteristic of high quality/acidity MCM-22 zeolites, with prominent bands of acidic OH groups at 3615 cm^{-1} (Fig. 4). The intensities of these bands are similar for all samples, as are the values of BAS concentrations (850 to 970 μmol g^{-1}). The measured acidity is lower than that which may be expected from the Si/Al ratio obtained by XRF due to the formation of LAS and non-acidic Al–OH groups. The presented spectra show only slight differences among the samples, such as the intensity of the band of terminal (3750 cm^{-1}) or geminal (3733 cm^{-1}) silanol groups. It does not influence the acidic properties of the materials. As indicated by the UV-vis spectra in Fig. 6, some of the incorporated cerium is tetravalent, thus forming only siloxane bridges Si–O–Ce^{4+} with no OH group attached. Extraframework Ce–OH groups, if present, should give rise to the specific IR maximum in the region 3660–3675 cm^{-1}, as reported in the literature.[33,34] The position of this band is very close to the one, usually reported for non-acidic Al–OH groups (3660 to 3680 cm^{-1}), which is also present in our samples (Fig. 4 and ESI† Fig. S2). Such Ce–OH groups are acidic and should disappear after pyridine adsorption,[35] which does not occur in our case (ESI,† Fig. S2). One should also expect that the intensity of the band at 3665 cm^{-1} would increase after cerium introduction, while it can be seen that this maximum is less intense for cerium-containing samples. Even when cerium was introduced as the exchangeable cation (sample denoted as Ce-A-no acid-IEZ-Ce), we did not observe the formation of an additional maximum at 3665 cm^{-1} (ESI,† Fig. S3).

5. Ce incorporation based on IR and UV-vis

The nature of Lewis acid centres was probed by adsorption of CO at −100 °C. It did not show the presence of significant

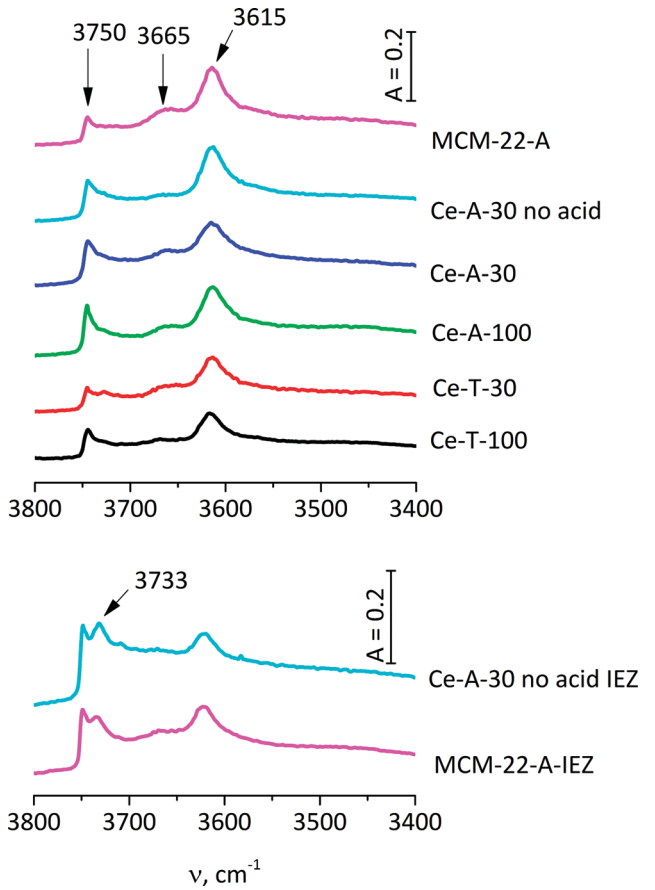

Fig. 4 IR spectra in the OH region for Ce-MWW zeolites activated under vacuum at 470 °C. Spectra at RT, normalized to 10 mg of sample.

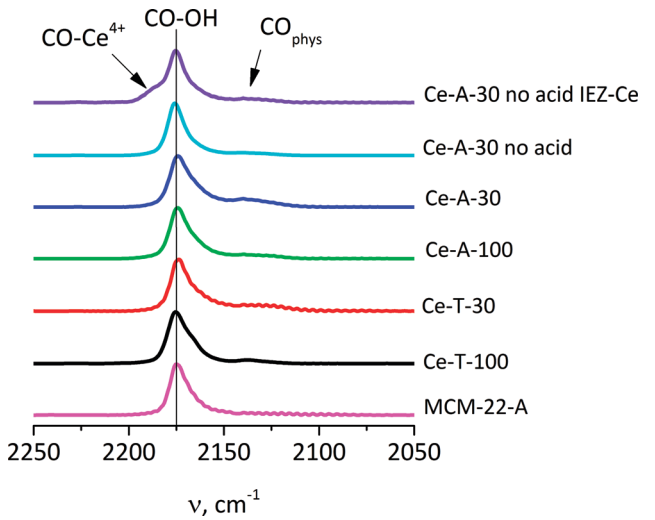

Fig. 5 IR spectra of CO adsorbed at −100 °C in the MWW zeolites under study. Spectra normalized to the intensity of CO–OH and at 2174 cm^{-1}.

amounts of extraframework cerium cations or cerium oxides. This is consistent with the incorporation of the majority of Ce inside the MWW framework, presumably in the tetrahedral positions, as suggested in the previous work.[23] The spectra, shown in Fig. 5, indicate that most of the cerium present is incorporated in the MWW structure. This is concluded because after CO adsorption, the main spectral feature in the range of 2250–2050 cm^{-1} is the band at 2174 cm^{-1}, which is characteristic of CO bonded to acidic OH groups: Si–OH–Al or Si–OH–Ce^{3+}. For comparison, the spectrum of CO adsorbed in the cerium-exchanged MWW-IEZ material is presented, with a distinct maximum at *ca.* 2190 cm^{-1}, characteristic of CO adsorbed at Ce^{4+} at exchangeable positions.

The spectra recorded after pyridine adsorption (ESI,† Fig. S1) show for all framework-substituted samples only the maxima, characteristic of pyridine adsorbed on BAS (1545 cm^{-1}), LAS (1454 cm^{-1}) and silanol groups (1445 cm^{-1}). Only in the case of the cerium-exchanged MCM-56 sample,[22] where cerium was introduced as the exchangeable cation, two new maxima appear, characteristic of pyridine adsorbed on cerium cations – at 1594 cm^{-1} (C–C stretching vibration of the pyridine ring) and at 1442 cm^{-1} (C–N stretching vibration of the pyridine ring). This experiment shows that cerium in framework-substituted zeolites is not detected by pyridine as the extraframework cation.

UV-vis spectra were obtained to evaluate both the chemical environment (coordination) and oxidation state of cerium in the studied MWW zeolites. The as-synthesized materials obtained by our group, both with TEOS and with solid silica, showed prominent bands at 220 and 280 nm, which are assigned to Ce^{3+} and Ce^{4+} cations, respectively, in tetrahedral coordination, and thus are considered incorporated into the zeolite frameworks. Wu *et al.* reported 'a broad absorption band at 300 nm due to the presence of well-dispersed tetracoordinated Ce(IV) centers and a weak shoulder at 250 nm assignable to tetrahedral Ce(III) sites'[23] based on the earlier study.[36] Our UV-vis spectra show a higher contribution of tetrahedrally coordinated Ce^{3+} than that in the work of Wu.

UV-vis spectra were obtained additionally for samples that were calcined in air at 550 °C. No significant changes were observed in the shape or intensity of the bands characteristic of both Ce^{3+} and Ce^{4+}, which again suggest that, in all cases, cerium remained incorporated into the framework. When cerium is introduced into the zeolite as the exchangeable cation, the UV-vis spectrum changes considerably after calcination due to dehydration of the cation and formation of small cerium oxide clusters. The spectrum of cerium-exchanged MCM-56 (chosen because it accommodates more cerium than MCM-22 zeolite) zeolite is shown as an example (Fig. 6).

6. The preparation of expanded Ce-MWW-IEZ by interlayer silylation

Calcination converts layered zeolite precursors, such as MCM-22P, into their corresponding frameworks by contraction and layer condensation. It is also possible to produce an expanded IEZ (Interlayer Expanded Zeolite) material by silylation with dialkyldialkoxysilanes, in which additional $SiOR_2$ links, R = alkyl or OH, are inserted between the layers. In the case of MCM-22P, it caused enlargement of the interlayer pores from a 10-ring to an effective 12-ring with an increase

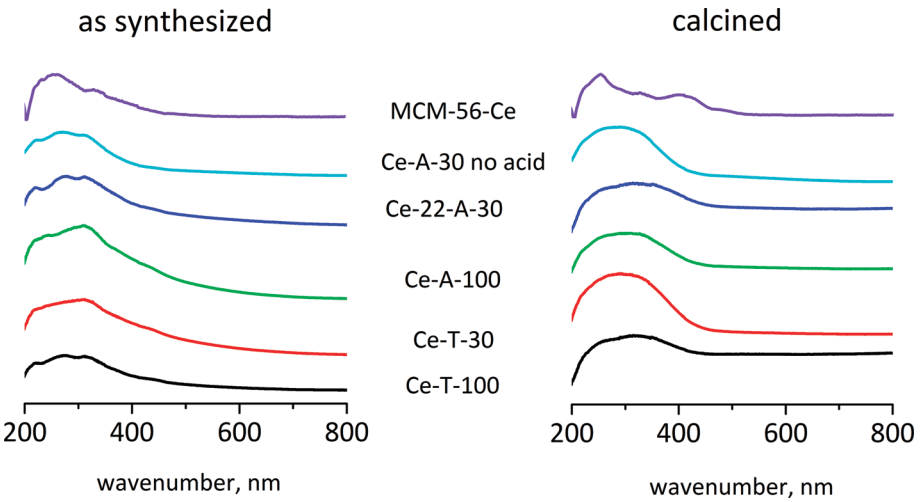

Fig. 6 DRS-UV-Vis spectra of MWW zeolites as-synthesized and calcined in air at 550 °C.

in the interlayer distance by about 0.2 nm in comparison to the MWW framework. This can translate into significant practical benefits as exemplified by the increased capacity for uptake of Ce by exchange, which rose over two-fold. As a result of this, the Ce-exchanged MWW-IEZ started showing the ability to oxidize CO to CO_2 at room temperature, which the Ce-MWW was lacking.[22] This may not have an immediate value in practice but is indicative of the potential presented by modification of layered zeolites into expanded derivatives.

This presents two types of Ln-MWW materials with cations built in during synthesis and exchanged post-synthesis. At the same time, the expanded IEZ shows qualitative differences by enabling CO oxidation upon Ce exchange. From this perspective, one can consider various possibilities involving starting MCM-22P materials with and without initial Ce, their Ce exchange alone, conversion of both into the IEZ form and again evaluation of Ce exchange. We have examined some of these permutations with the purpose of determining the effect of various treatments on the textural properties and the state of Ce based on its oxidation of CO.

The XRD pattern shown in Fig. 1 indicates the successful silylation of the Ce-MCM-22 precursor to form the IEZ product. It is noteworthy that the precursor had high Al content, which in the case of the normal MCM-22P results in decreased efficiency of IEZ formation. In other words, Ce-MCM-22P can be made into IEZ in a lower range of Si/Al ratios, whereas regular MCM-22P cannot. On the other hand, the final Al content was not much different compared to that in typical silylations as a result of Al leaching, which is common in highly acidic environments. The Ce content also drops considerably. The textural properties of the MWW-IEZ zeolites were studied in detail by the QE-TPDA method and are discussed in the section below.

The enlargement of the interlayer pores from 10-ring to 12-ring enhances the accessibility of the intralayer OH groups to bulky molecules, such as pivalonitrile (PN), which is a molecule with a large *tert*-butyl group. Acidic Si–OH–Al groups in the standard 3D MCM-22 zeolite are hardly accessible to this molecule – the intensity of the Si–OH–Al band is almost unchanged after PN adsorption (Fig. 7). For the IEZ forms, all OH groups should become accessible, thus the interaction with pivalonitrile is a good measure of whether the expansion is complete or not. It can be noted that for both IEZ materials (both with and without cerium), the intensity of the band of Si–OH–Al groups decreased after PN adsorption and the band of the remaining OH groups is less intense for the cerium-IEZ form, indicating a greater extent of silylation. This is also in agreement with the corresponding XRD patterns.

7. Porosity

The pore characteristics of the prepared zeolite samples have been studied by the QE-TPDA method (quasi-equilibrated temperature-programmed desorption and adsorption) in comparison to the standard nitrogen adsorption method. QE-TPDA is a valuable complementary tool for porosity characterization since, by using various hydrocarbons as probe

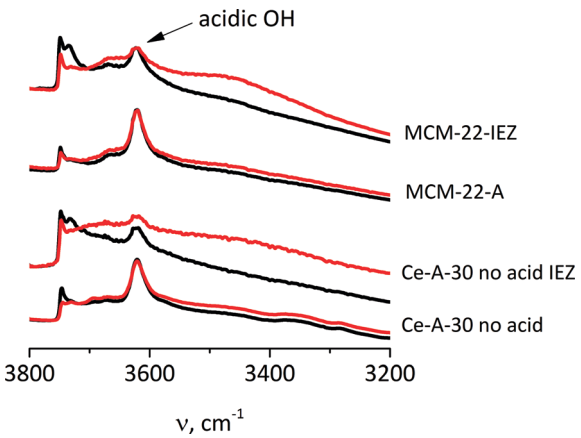

Fig. 7 IR spectra of OH groups after pivalonitrile adsorption in MWW and the corresponding IEZ-MWW zeolites. Black spectra – activated samples before pivalonitrile adsorption, red spectra – after pivalonitrile adsorption and subsequent evacuation for 5 minutes at RT (for color coding, please refer to the online version of the paper).

molecules, it reveals additional details associated with pores and their internal environment in response to the dimensions/shape of various sorbate molecules. Fig. 8 presents the N_2 adsorption–desorption isotherms observed for all studied MCM-22 materials. The values of specific surface areas and pore volumes determined from the N_2 adsorption data are listed in Table 3 together with the pore volumes calculated from the thermodesorption data for hexane, cyclohexane and nonane. The corresponding QE-TPDA profiles are shown in Fig. 9 and 10.

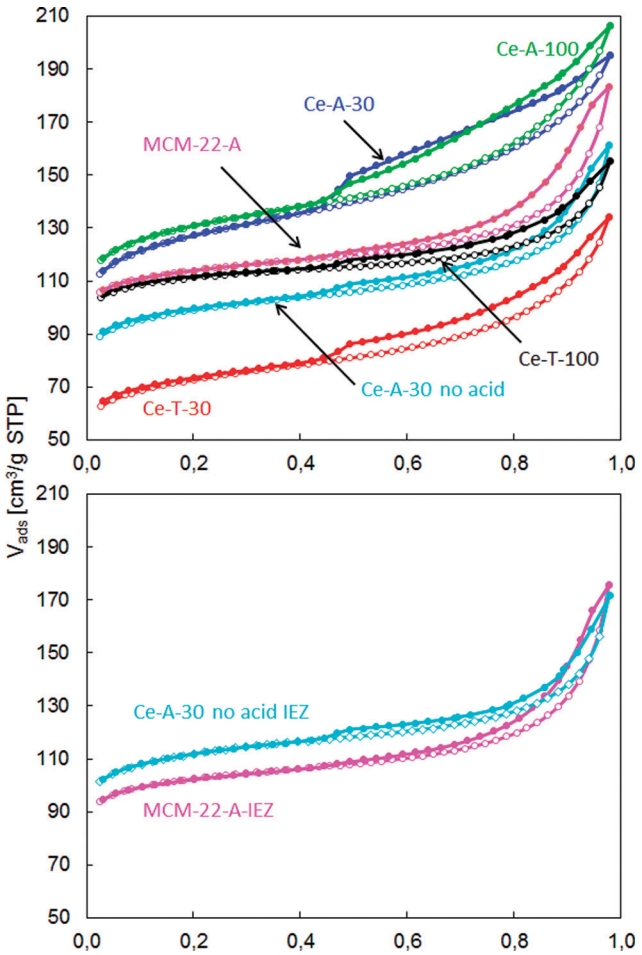

Fig. 8 N_2 adsorption isotherms of the zeolites under study.

The N_2 adsorption isotherms are typical for microporous materials exhibiting a plate-like morphology of the crystals. The values of the micropore volume are quite similar for most of the studied zeolites (0.13–0.17 cm^3 g^{-1}, except that of 0.09 cm^3 g^{-1} for Ce-T-30), close to those usually reported for MCM-22 (0.17–0.20 cm^3 g^{-1}).[30,37,38]

The results of the QE-TPDA measurements are presented in Fig. 9 and 10 as profiles of specific sorption rate (ssr, [μmol g^{-1} s^{-1}]) *vs.* temperature. They consist of desorption maxima observed during heating and adsorption minima observed while cooling the sample. They were calculated by averaging raw experimental data from at least 3 desorption–adsorption cycles.

The QE-TPDA measurements of hexane and cyclohexane (Fig. 9), performed using a low partial pressure of the adsorptive in the carrier gas ($p/p_{sat} < 0.05$), allowed the selective probing of the micropores. The profiles of hexane (Fig. 9, left panes), exhibiting one broad desorption maximum, are in agreement with the previously reported data.[30] The corresponding pore volume values, which are close to the N_2 adsorption results, corroborate the microporosity of the studied zeolites. The profiles and pore volumes found for the interlayer expanded zeolites (IEZ) indicate their enhanced microporosity. In the QE-TPDA profiles of cyclohexane, one desorption maximum was observed for the standard MCM-22 zeolites, but two desorption maxima were detected for the IEZ ones (Fig. 9, right panes). These results indicate considerably increased accessibility of the MWW micropores for adsorption of larger molecules upon silylation producing the IEZ derivative.

The QE-TPDA profiles of nonane (Fig. 10) were measured using He gas saturated with the hydrocarbon vapor and they contain features related to both micropores and mesopores.[31] The low-temperature maxima (25–80 °C), differing in shape and intensity, confirm the differences in the external surface area and interparticle mesoporosity found for the studied zeolites in their N_2 adsorption isotherms. The high-temperature maxima, similar to those observed in the case of hexane, corroborate the conclusions concerning the different microporosities of the standard and interlayer expanded zeolites.

Table 3 Porosity parameters calculated from the N_2 adsorption data and QE-TPDA profiles of hydrocarbons

	S (N_2 ads), m^2 g^{-1}		V_{pore} (N_2 ads), cm^3 g^{-1}		V_{pore} (QE-TPDA), cm^3 g^{-1}		
Sample	BET	Ext.[a]	Micro[a]	Meso[b]	Hexane	Cyclohexane	LT nonane[c]
Ce-T-100	358	23	0.16	0.08	—	—	—
Ce-T-30	240	59	0.09	0.12	0.11	0.03	0.08
Ce-A-100	426	73	0.17	0.15	—	—	—
Ce-A-30	417	88	0.16	0.14	0.13	0.05	0.08
Ce-A-30-no acid	322	47	0.13	0.12	0.13	0.02	0.05
Ce-A-30-no acid-IEZ	363	39	0.16	0.11	0.16	0.09	0.06
MCM-22-A	368	41	0.16	0.12	0.14	0.06	0.04
MCM-22-A-IEZ	331	38	0.14	0.13	0.12	0.06	0.08

[a] Calculated using the *t*-plot method. [b] Calculated as $V_{total} - V_{micro}$. [c] Calculated for the low-temperature (LT) maxima (30–80 °C), corresponding to desorption from the external surface and mesopores.

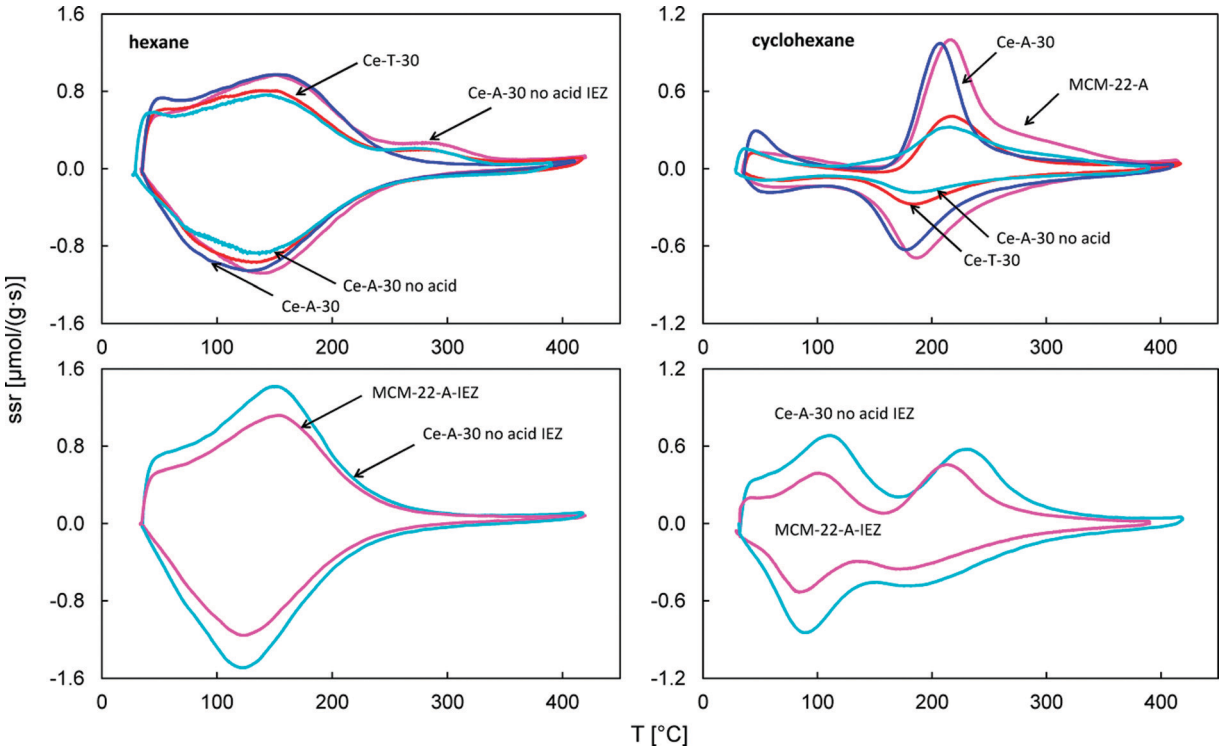

Fig. 9 QE-TPDA profiles of hexane (left) and cyclohexane (right).

8. CO oxidation activity

The CO oxidation ability at room temperature was observed with Ce exchanged into MCM-22-IEZ but not into MCM-22, which is probably due to the higher content of cerium incorporated in the former. The framework-substituted Ce-MCM-22 materials did not show any activity in that regard and the interlayer expanded form (IEZ form) was also inactive, at least without additional Ce exchange. This contrast between the Ce-exchanged MWW-IEZ, which shows high CO oxidation activity, and the Ce-MCM-22 obtained by direct synthesis, which is inert despite containing more than two times the amount of Ce, indicates the completely different nature of the metal atoms in both samples. The difference is attributed to Ce in-the-framework in contrast to being external such as those in the exchanged MCM-22 and MCM-22-IEZ materials. The framework-substituted Ce atoms appear to be dispersed and are clearly different from the exchanged extraframework species. As the next step, the inactive Ce-MWW-IEZ was ion-exchanged with cerium to see if it becomes active for CO oxidation. Just like its counterpart – the cerium-exchanged MWW-IEZ, the Ce exchanged Ce-MCM-22 became active for CO-to-CO_2 oxidation at room temperature. This underscores the difference between these two methods of Ce incorporation into MCM-22 and may be applicable to other zeolites too. The exchange of Ce into regular, not IEZ expanded, Ce-MCM-22 did not induce CO oxidation activity, exactly as observed with Ce exchange into MCM-22. This indicates that some expansion of the interlayer distance is essential to obtain an active form of Ce by exchange into a zeolite framework.

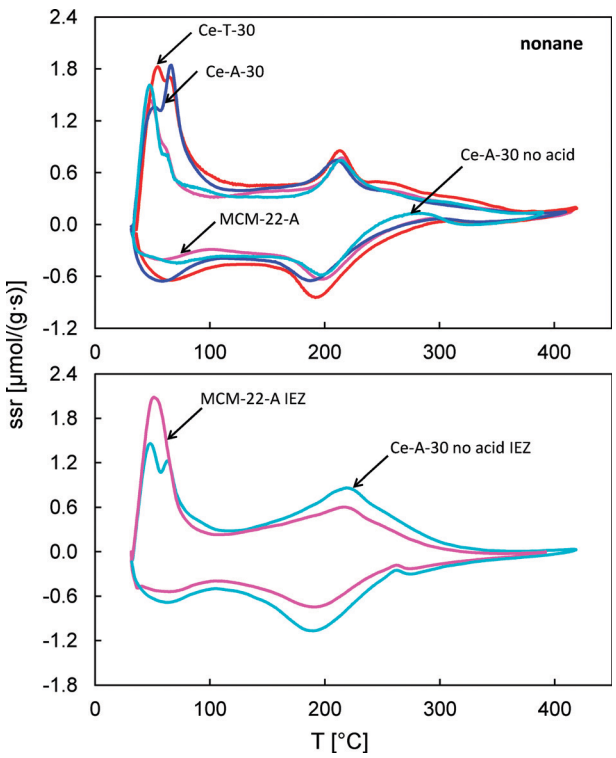

Fig. 10 QE-TPDA profiles of nonane.

Summary and outlook

The preparation of Ln-MCM-22 by direct synthesis is an important advancement, not only as it concerns the MWW

family but also because of its potential for extension to other frameworks and various metal elements. The present work shows that a solid silica source can produce MCM-22P with properties comparable to those of valuable materials produced with TEOS. This has implication for the underlying formation mechanism and also offers an attractive method for convenient economical preparation.

The conclusions from XRD, spectroscopic and textural studies are that both TEOS and fumed silica produced highly crystalline MCM-22 containing cerium in 3+ and 4+ oxidation states with no evidence of location in extraframework positions. Ce incorporation reduces the concentration of BAS but it remains high. The ratio of BAS to LAS is more than 10 : 1 in most cases.

Modification of the MWW framework is of great interest for catalysis because of the remarkable activity of the base zeolite and its use in commercial processes like aromatic alkylations. The described Ce-MWW materials, both framework-substituted and exchanged, have shown activity which is very relevant for catalysis. The former exhibited enhancement in acid catalysis (*n*-heptane isomerization). The latter showed CO oxidation at room temperature but a viable catalytic process will require an elevated temperature for faster kinetics and to facilitate CO_2 desorption. Ce addition modifies the acidic properties of the MCM-22 zeolite as indicated by the FTIR measurement. This is expected to influence its performance in alkylation catalysis and can be tested by model reactions such as the Friedel–Crafts alkylation of benzene with benzyl alcohol,[39] which is planned as a follow-up. MCM-22 is also amenable to additional structural transformations like pillaring and delamination, which further modify its characteristics, especially increasing the accessibility of the layer surface. The corresponding lanthanide-substituted versions will be of great interest to explore and characterize, including their catalytic potential.

Acknowledgements

This work was financed with the funds from the Narodowe Centrum Nauki provided on the basis of decision number DEC-2011/03/B/ST5/01551. The IR measurements were carried out with the equipment purchased thanks to the financial support of the European Regional Development Fund in the framework of the Polish Innovation Economy Operational Program (contract no. POIG.02.01.00-12-023/08).

References

1 D. W. Breck, *Zeolite Molecular Sieves: Structure, Chemistry, and Use*, Wiley, New York, 1973.
2 A. F. Masters and T. Maschmeyer, *Microporous Mesoporous Mater.*, 2011, **142**, 423–438.
3 C. Baerlocher, L. B. McCusker and D. H. Olson, *Atlas of Zeolite Framework Types*, Elsevier, Amsterdam, 2007, (also: http://www.iza-structure.org/).
4 J. V. Smith, *Chem. Rev.*, 1988, **88**, 149–182.
5 J. Cejka, A. Corma and S. Zones, *Zeolites and Catalysis*, Wiley, Weinheim, 2010.
6 W. O. Haag, R. M. Lago and P. B. Weisz, *Nature*, 1984, **309**, 589–591.
7 I. Fechete, Y. Wang and J. C. Védrine, *Catal. Today*, 2012, **189**, 2–27.
8 O. Deutschmann, H. Knözinger, K. Kochloefl and T. Turek, in *Ullmann's Encyclopedia of Industrial Chemistry*, Wiley, Weinheim, 2009.
9 J. Weitkamp and L. Puppe, *Catalysis and Zeolites: Fundamentals and Applications*, Springer, Berlin, 1999.
10 S. I. Zones, *Microporous Mesoporous Mater.*, 2011, **144**, 1–8.
11 G. Bellussi, A. Carati, C. Rizzo and R. Millini, *Catal. Sci. Technol.*, 2013, **3**, 833–857.
12 G. Perego, R. Millini and G. Bellussi, in *Synthesis*, ed. H. G. Karge and J. Weitkamp, Springer-Verlag, Berlin, 1998, ch. 7, pp. 187–228.
13 M. G. Clerici, in *Metal Oxide Catalysis*, ed. S. D. Jackson and J. S. J. Hargreaves, Wiley, Weinheim, 2009, vol. 2, pp. 705–754.
14 G. Bellussi and V. Fattore, *Stud. Surf. Sci. Catal.*, 1991, **69**, 79–92.
15 C. Hess, in *Comprehensive Inorganic Chemistry II*, ed. J. Reedijk and K. Poeppelmeier, Elsevier, Oxford, 2013, vol. 7, pp. 231–245.
16 M. G. Clerici and M. E. Domine, in *Liquid Phase Oxidation via Heterogeneous Catalysis*, Wiley, Weinheim, 2013, pp. 21–93.
17 L. Nemeth and S. R. Bare, *Adv. Catal.*, 2014, **57**, 1–97.
18 R. Szostak, *Molecular Sieves: Principles of Synthesis and Identification*, Blackie Academic and Professional, London, 1998.
19 E. F. Sousa-Aguiar, F. E. Trigueiro and F. M. Z. Zotin, *Catal. Today*, 2013, **218–219**, 115–122.
20 C. J. Plank, E. J. Rosinski and W. P. Hawthorne, *Ind. Eng. Chem. Prod. Res. Dev.*, 1964, **3**, 165–169.
21 C. Martínez and A. Corma, *Coord. Chem. Rev.*, 2011, **255**, 1558–1580.
22 W. J. Roth, W. Makowski, B. Marszalek, P. Michorczyk, W. Skuza and B. Gil, *J. Mater. Chem. A*, 2014, **2**, 15722–15725.
23 Y. Wu, J. Wang, P. Liu, W. Zhang, J. Gu and X. Wang, *J. Am. Chem. Soc.*, 2010, **132**, 17989–17991.
24 M. E. Leonowicz, J. A. Lawton, S. L. Lawton and M. K. Rubin, *Science*, 1994, **264**, 1910–1913.
25 T. F. Degnan, Jr., C. M. Smith and C. R. Venkat, *Appl. Catal., A*, 2001, **221**, 283–294.
26 J. C. Cheng, T. F. Degnan, J. S. Beck, Y. Y. Huang, M. Kalyanaraman, J. A. Kowalski, C. A. Loehr and D. N. Mazzone, *Stud. Surf. Sci. Catal.*, 1999, **121**, 53–60.
27 W. J. Roth, B. Gil and B. Marszalek, *Catal. Today*, 2014, **227**, 9–14.
28 P. Wu, J. F. Ruan, L. L. Wang, L. L. Wu, Y. Wang, Y. M. Liu, W. B. Fan, M. Y. He, O. Terasaki and T. Tatsumi, *J. Am. Chem. Soc.*, 2008, **130**, 8178–8187.
29 B. Gil, B. Marszałek, A. Micek-Ilnicka and Z. Olejniczak, *Top. Catal.*, 2010, **53**, 1340–1348.
30 W. Makowski, K. Mlekodaj, B. Gil, W. J. Roth, B. Marszałek, M. Kubu, P. Hudec, A. Smiešková and M. Horňáček, *Dalton Trans.*, 2014, **43**, 10574–10583.

31 W. Makowski and P. Kuśtrowski, *Microporous Mesoporous Mater.*, 2007, **102**, 283–289.
32 E. F. Sousa-Aguiar, V. L. D. Camorim, F. M. Z. Zotin and R. L. C. Dos Santos, *Microporous Mesoporous Mater.*, 1998, **25**, 25–34.
33 C. R. Moreira, M. M. Pereira, X. Alcobé, N. Homs, J. Llorca, J. L. G. Fierro and P. Ramírez de la Piscina, *Microporous Mesoporous Mater.*, 2007, **100**, 276–286.
34 L. D. Borges, N. N. Moura, A. A. Costa, P. R. S. Braga, J. A. Dias, S. C. L. Dias, J. L. De MacEdo and G. F. Ghesti, *Appl. Catal., A*, 2013, **450**, 114–119.
35 A. Guzman, I. Zuazo, A. Feller, R. Olindo, C. Sievers and J. A. Lercher, *Microporous Mesoporous Mater.*, 2005, **83**, 309–318.
36 S. C. Laha, P. Mukherjee, S. R. Sainkar and R. Kumar, *J. Catal.*, 2002, **207**, 213–223.
37 A. Zukal and M. Kubů, *Dalton Trans.*, 2014, **43**, 10558–10565.
38 C. Delitala, M. D. Alba, A. I. Becerro, D. Delpiano, D. Meloni, E. Musu and I. Ferino, *Microporous Mesoporous Mater.*, 2009, **118**, 1–10.
39 H. Y. Luo, V. K. Michaelis, S. Hodges, R. G. Griffin and Y. Román-Leshkov, *Chem. Sci.*, 2015, **6**, 6320–6324.